Demonstration of the Antitumor Activity of the iNKT Agonist ABX196, a Novel Enhancer of Cancer Immunotherapy, in Melanoma and Hepatocarcinoma Mouse Models

Didier Scherrer[1], Noel Barrett[2], Luc Teyton[3], Tillman Pearce[2], Josianne Nitcheu[4], Philippe Pouletty[4], Julien Santo[1], and Hartmut J. Ehrlich[4]

ABSTRACT

Immune checkpoint blockers (ICB) provide a promising approach to antitumor immunotherapy through blockade of immunosuppressive pathways. The synthetic glycolipid, ABX196, is a potent stimulator of invariant natural killer T cells (iNKT), a small subset of regulatory lymphocytes, which are powerful enhancers of immunity when activated. ABX196 was investigated alone and in combination with chemotherapy and ICBs in a melanoma B16F10 tumor cell-bearing and an orthotopic Hepa 1–6 hepatocarcinoma (HCC) cell-bearing C57BL/6 mice model. In the melanoma model, immune response evaluation included immunofluorescence staining and detection by flow cytometry to identify anti-CD45, anti-CD8, anti-CD4, anti-CD3, anti-CD19, anti-FoxP3, CD1d tetramer, and anti—programmed cell death protein 1 (PD-1) markers. Analysis by MRI, liver weight, and IHC staining to detect CD4, CD8, F4/80, PD-1, programmed death-ligand 1, Ki67, and FoxP3 markers were used to measure antitumor response in the HCC model. Combination treatment with ABX196 and anti–PD-1 resulted in significant synergistic antitumor effects, reflected by the increase of $CD8^+$ cells in the tumor and an increased ratio of $CD8^+$ effector cells to $FoxP3^+$ regulatory T cells (Treg) in mice with melanomas. ABX196 monotherapy and combination therapy resulted in antitumor effects in the HCC model. No significant differences in survival were demonstrated between monotherapy and combination therapy due to high response levels with either treatment. A synergistic combination effect was apparent when IFNγ was measured in peripheral blood, indicating sustained activation of iNKT cells. In both models, the antitumor effects were associated with a generation of a more advantageous T-effector to Treg cell ratio within the tumor, which could lead to in the proliferation and accumulation of cells that would otherwise be anergized.

Synopsis: Using melanoma and HCC tumor models in mice, this study demonstrates the potential of ABX196, alone and in combination with anti–PD-1 antibody, as a novel strategy to overcome the immunosuppressive microenvironment and to produce antitumor activity.

Introduction

Liver cancer is the fourth leading cause of global cancer-related deaths and is the seventh most frequently diagnosed cancer worldwide with an incidence of one million cases globally in 2016 (1, 2). The most common form of liver cancer worldwide is hepatocellular carcinoma (HCC; ref. 3). Although HCC has several etiologies, which may contribute to its heterogeneous nature, immunotherapy provides a promising treatment option, as HCC is frequently associated with chronic inflammation (4). Recent evidence demonstrates antitumor immunity in HCC such as tumor-associated antigens recognized by cytotoxic T cells and reports of spontaneous immune-mediated regression (4). Moreover, tumor-specific T cells can prevent the development of cancer through cytotoxic activity against tumor cells, and the release of pro-inflammatory cytokines that promote an antitumor response (5–7). However, HCC and the liver may potentiate an immunosuppressive environment through suppression of pro-inflammatory effector T cells (4, 8). HCC-modulated immunosuppression can be achieved by multiple mechanisms, including enhancement of regulatory T cells (Treg), and/or the suppressive effects of anti-inflammatory cytokines, and/or co-inhibitory molecules (9, 10). One of the most promising approaches to activate therapeutic antitumor therapy is the blockade of these pathways by use of immune checkpoint blockers (ICB; refs. 11, 12). Co-inhibitory molecules such as programmed cell death protein 1 (PD-1) and cytotoxic T-lymphocyte–associated protein (CTLA)-4 play an important role in tumor-induced immunosuppression by inhibiting activation of T cells. Antibodies targeting these inhibitors demonstrate interference with these suppressive signaling events and are approved for treatment of a variety of cancers (11, 13, 14). However, these valuable immunotherapies induce durable responses in only 20% to 30% of patients (15), so there is a need to enhance their activity.

We studied ABX196, a novel synthetic glycolipid analog of the parental compound α-galactosylceramide (α-GalCer), for immunomodulatory activities, that has been obtained according to a previously published procedure (16). ABX196 was selected from a library of about 200 variants of α-GalCer that explored the importance of the three components of glycosylceramides: headgroup, acyl chain, and sphingosine. ABX196 differs from α-GalCer by the presence of a phytosphingosine instead of a sphingosine, and an amino group at position C6 of the galactosyl headgroup (Supplementary Fig. S1). This glycolipid family is a highly potent stimulator of a small subset of regulatory

[1]Abivax, Montpellier, France. [2]Independent Consultant, c/o Abivax, Paris, France. [3]Department of Immunology and Microbial Science, The Scripps Research Institute, La Jolla, California. [4]Abivax, Paris, France.

Corresponding Author: Julien Santo, Abivax, 1919 Route de Mende, Montpellier 34293, France. Phone: 434-359-596; E-mail: julien.santo@abivax.com

Mol Cancer Ther 2022;21:1788–97

doi: 10.1158/1535-7163.MCT-22-0183

lymphocytes called invariant natural killer T cells (iNKT; refs. 17, 18). iNKT cells are powerful enhancers of immunity, which can be activated in both antigen-dependent and -independent manners, leading to production of Th1 and Th2 cytokines (18). In particular, $CD4^+$ iNKT cells produce both Th1 and Th2 cytokines, whereas CD4−iNKTs predominantly produce Th1 cytokines, IFNγ and TNFα (19). Accordingly, the pro-inflammatory and immunomodulatory features of iNKT cells demonstrate their functional adaptability (18). iNKT cells also exhibit cytolytic functionality through high expression levels of granzyme B, perforin, and Fas Ligand (FasL) and are important for activation of several immune cell types, including natural killer (NK) cells, conventional $CD4^+$ and $CD8^+$ T cells, macrophages, and B cells (20). In a murine study, iNKT cells demonstrate influence of the adaptive immune response through enhanced B-cell memory and improved antibody titers following iNKT activation (21). Consequently, iNKT cells have a significant effect on the immune response to infectious disease, allergy, autoimmunity, and tumor surveillance (18).

This study investigates the potential of ABX196 as a cancer immunotherapy alone and in combination with chemotherapy and ICBs in melanoma and HCC tumor models in mice.

Materials and Methods

Tumor models

Experiments for the melanoma model study were performed by Explicyte (Bordeaux, France) and animals were housed in the animal facility, Animalerie Mutualisée Bordeaux 1, which received approval B33–522–22 from the Bordeaux Ethical Committee (CEEA50 Comité d'éthique de Bordeaux). C57BL/6 mice were purchased from Charles River Laboratories, L'Arbresle, France. Melanoma B16F10 (ATCC CRL-6475) cells (1×10^6 cells/100 μL) were implanted subcutaneously in the right flank of C57BL/6 immunocompetent mice (8-week-old females). Tumor volume, survival, and body weight of the animals were measured and recorded 3 times per week. A tumor volume > 2,000 mm^3 or a weight loss > 15% relative to the initial weight of the animal were considered as endpoints and the animal was sacrificed.

For the HCC model study, experiments were performed by Oncodesign (Dijon, France) and all animal procedures were submitted to the Animal Care and Use Committee of Oncodesign (Oncomet) and approved by French authorities (CNREEA agreement N° 91). C57BL/6 mice were purchased from Janvier Labs, Le Genest-Saint-Isle, France. Hepa 1–6 cells (ATCC CRL-1830; 1×10^6 cells/50 μL) were transplanted via intrasplenic injection into 100 C57BL/6 mice (aged 5–6 weeks old).

Hepatic cellular carcinoma model

After implantation, mice were randomized at day 0 into 6 groups (12–13 mice *per* group) as follows: (i) intravenous injection with control vehicle on day 5, (ii) 100 ng ABX196 i.v. on day 5, (iii) 100 mg/kg sorafenib (the current standard of treatment care; ref. 22) oral gavage daily for 21 consecutive days, (iv) 100 ng ABX196 i.v. on day 5 and 100 mg/kg sorafenib oral gavage daily for 21 consecutive days, (v) 10 mg/kg anti–PD-1 antibody intraperitoneal on days 7, 10, 14, and 17, and (vi) 100 ng ABX196 i.v. on Day 5 and 10 mg/kg anti–PD-1 antibody intraperitoneal on days 7, 10, 14, and 17 (**Fig. 1A**). All doses of ABX196 were administered intravenously via the tail vein at the dose of 100 ng per animal. Anti–PD-1 antibody was administered at a dose of 10 mg/kg and sorafenib was administered at a dose of 100 mg/kg.

For immune marker analysis by IHC staining, animals were sacrificed at the end of the study. Tumor and liver tissue were sliced into 4-mm sections and fixed in 4% neutral buffered formalin for 24 to 48 hours, and then embedded in paraffin (Histosec, Merck, Darmstadt, Germany). Three animals *per* group were chosen randomly for IHC staining with 1 section (thickness 3–5 μm) *per* group deposited on Superfrost+ slides. Staining was performed using hematoxylin and eosin (H&E) stain and automated platforms to detect markers CD4, CD8, F4/80, PD-1, programmed death-ligand 1 (PD-L1), KI67, and FoxP3. The slides were digitalized with the Nanozoomer scanner (Hamamatsu) in conditions of bright field and fluorescence with the objective ×20 without Z stack. As tumor grafts were not effective for all animals, the analyses were only performed on the sections with tumor tissue. For animals with tumor, each slide contained between 4 and 12 sections, and the section with the larger tumor tissue was analyzed. Immunofluorescent staining of liver tissue was performed with antibody specific for Ki-67, an antigen associated with cell proliferation (23) and which is often correlated with the clinical course of cancer (24). The surface of total and stained tissue was quantified using an in-house internally validated image analysis algorithm (HistoQuantif). According to the surface measured for each staining, a percentage of stained surface was calculated for each marker in each treatment group.

Antitumor activity was monitored through MRI of the liver, liver weight, and mouse survival. Five animals *per* group were imaged using MRI at days 19 and 20. All imaging experiments were performed on a 4.7T horizontal magnet (PharmaScan, Bruker Biospin GmbH, Germany) equipped with an actively shielded gradient system. All the MR images were acquired under ParaVision (PV5.1, Bruker Biospin) and analyzed under ImageJ using in-house written software. A semiquantitative analysis was performed by visual inspection of 20 consecutive images covering the liver to evaluate tumoral invasion and expressed as a percentage of invasion. All MR images were analyzed blind, in random order.

In addition, serum IFNγ was analyzed on day 3 (before tumor engraftment) and on day 9 (after first treatment and tumor engraftment).

Melanoma model

For assessment of antitumor efficacy, mice were randomized into 4 groups (control vehicle–treated group, anti–PD-1—treated group intraperitoneal administration, ABX196-treated group intravenous administration, ABX196 intravenously in combination with anti–PD-1 antibody intraperitoneal) with 14 mice *per* group (**Fig. 1B**). Following implantation at day 0, mice were injected with anti–PD-1 antibody intraperitoneal (100 μg in 100 μL) at day 6, 9, 12, 15, and 18; and 1 dose of ABX196 i.v. (100 ng in 100 μL) was administered via the tail vein at day 10 in the ABX196 group and combined ABX196/anti–PD-1 treatment group.

In addition, groups of 5 mice (identical to the groups described above) were used for immune profiling studies and sacrificed at day 11 after tumor implementation. Immune profiling was performed for tumoral tissue and peripheral lymphoid tissue to evaluate the immunologic response to the different treatment regimens. Following flow cytometry analyses, cells from the tumor, spleen and tumor-draining lymph nodes (TDLN) were extracted and processed for immunofluorescence staining.

For immune profiling by flow cytometry, groups of 6 mice were sacrificed at day 14 following tumor cell inoculation. The tumor, spleen, and TDLNs were retrieved, then homogenized and processed for immunofluorescence staining and detection by flow cytometry.

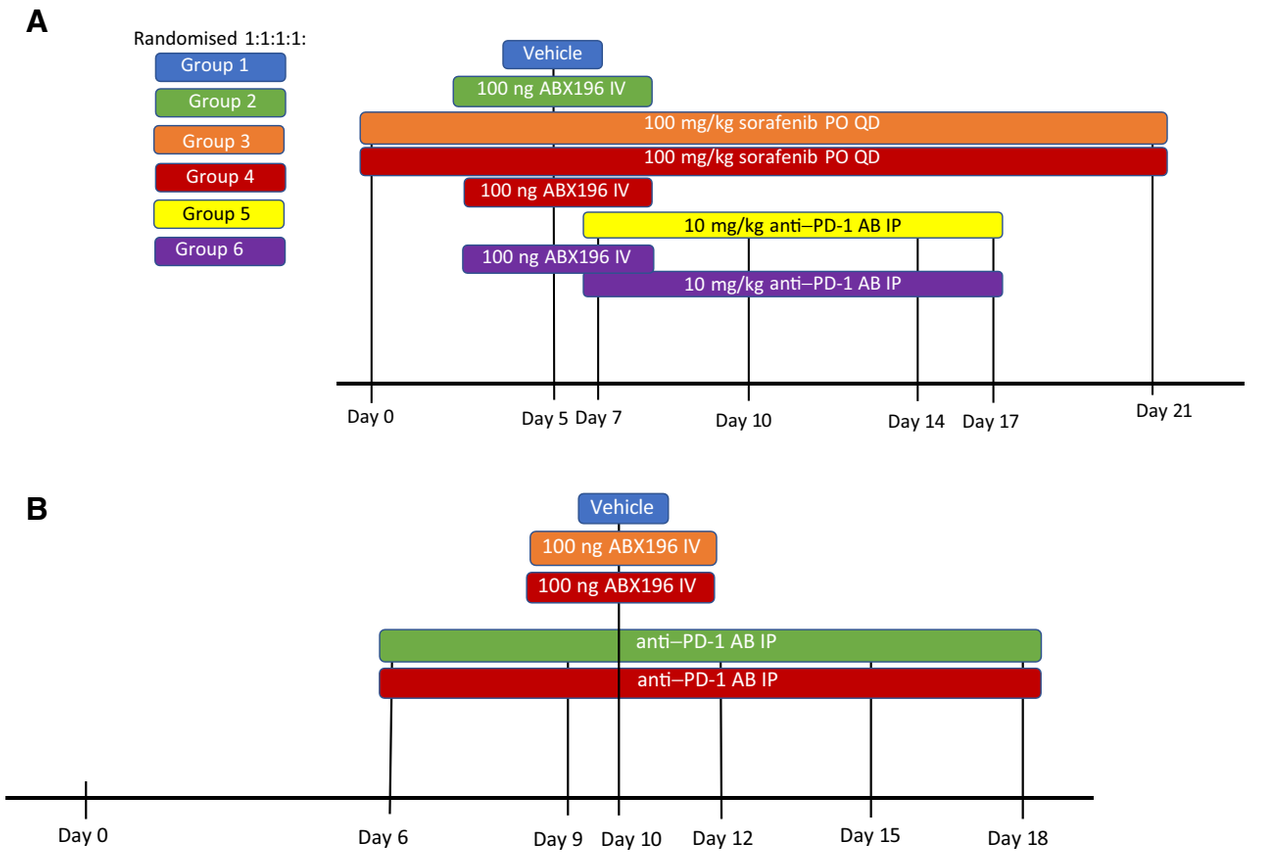

Figure 1.
Study design for hepatocellular tumor model (**A**) and melanoma tumor model (**B**).

Homogenate samples were stained for anti-CD45, anti-CD8, anti-CD4, anti-CD3, anti-CD19, anti-FoxP3 intracellular staining, CD1d tetramer, and anti–PD-1 markers. Antibodies were obtained from Miltenyi Biotec (Germany) except CD1d-aGalCer, which was obtained from ProImmune (United Kingdom).

Statistical analysis

All statistical analyses were performed using Graph Pad Prism 6 software. Log-rank (Mantel–Cox) test was performed for statistical analyses of mean tumor volume. Each test is described in the legends of figures and in the supplementary statistical tables.

Data availability statement

The data generated in this study are available upon request from the corresponding author.

Results

Antitumor response in a melanoma B16F10 tumor-bearing mice model

Treatment with ABX196 both alone and in combination with anti–PD-1 was evaluated for its capacity to induce and/or enhance the antitumor response in a melanoma B16F10 tumor-bearing mice model. Results from these analyses showed no significant effect of anti–PD-1 antibody for both tumor volume and survival. A transient effect was observed on tumor volume 15 days after ABX196 administration but was not significant versus control ($P = 0.054$). A significant synergistic effect of a combination of anti–PD-1 with ABX196 was observed for both tumor volume ($P < 0.05$ at day 15 versus control; $P < 0.01$ at day 15 and 17 compared with anti–PD-1 alone) and survival time ($P < 0.05$ vs. control, **Fig. 2**; Supplementary Table S1). Combined ABX196/anti–PD-1 treatment had a significant reduction in mean tumor volume at day 17 versus control ($P < 0.05$), versus ABX196 monotherapy ($P = 0.005$) and versus anti–PD-1 monotherapy ($P < 0.05$). ABX196 treatment alone and in combination with anti–PD-1 had a significant beneficial effect on survival versus control ($P < 0.05$ for both), whereas no significant difference was seen for anti–PD-1 treatment alone.

For immune profiling, results for $CD8^+$ cell measurement in spleen or TDLNs were comparable between the treatment and control groups. A slight increase in proportion of $CD8^+$ cells was seen in tumor-derived cells following combined ABX196/anti–PD-1 administration (**Fig. 3A**). Combined ABX196/anti–PD-1 treatment yielded the highest ratio of CD8 effector to FoxP3 Tregs in tumoral tissue, but there was no significant difference across groups (**Fig. 3B**).

Analysis by different regulatory cell populations investigated the underlying mechanism for the increase in $CD8^+$ cells in tumoral tissue. Compared with vehicle control, the concentration of $CD4^+$ Tregs ($PD\text{-}1^+/FoxP3^+$) in tumors decreased in this cell population following treatment with anti–PD-1, ABX196, or combined ABX196/anti–PD-1 treatment, with a significant effect observed after treatment with ABX196 ($P < 0.05$); no synergistic effect was obtained following

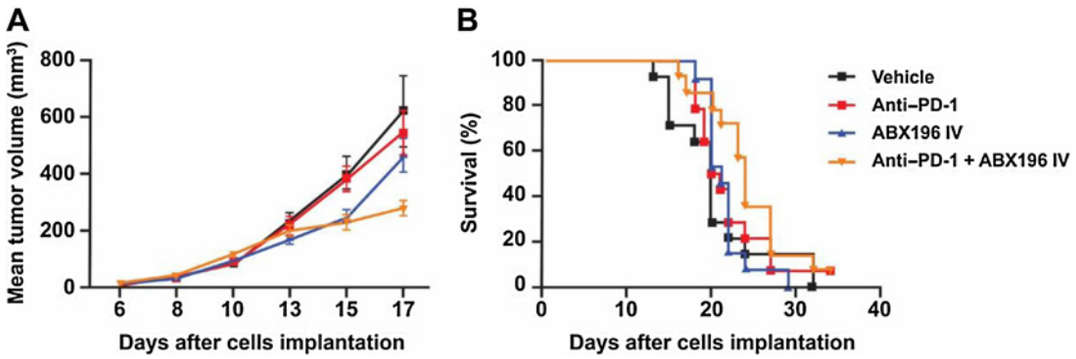

Figure 2.

Tumor regression and survival following administration of ABX196 ± anti–PD-1. **A,** Mean tumor volume ± SEM (mm^3) of B16F10–bearing mice exposed to vehicle ($n = 14$), to anti–PD-1 antibody alone ($n = 13$), to ABX196 ($n = 14$), or to combination of anti–PD-1 antibody and ABX196 ($n = 14$). **B,** Survival analysis of B16F10-bearing mice exposed to vehicle ($n = 14$), to anti–PD-1 antibody alone ($n = 13$), to ABX196 ($n = 14$), or to the combination of anti–PD-1 antibody and ABX196 ($n = 14$). Survival is represented as percentage of animals (%). A significant synergistic effect of a combination of anti–PD-1 with ABX196 was observed for both tumor volume ($P < 0.05$ at day 15 vs. control; $P < 0.01$ at day 15 and 17 compared with anti–PD-1 alone; mixed-effects model and a Dunnett multiple comparisons test) and survival time ($P < 0.05$ vs. control; see Supplementary Table S1 for details).

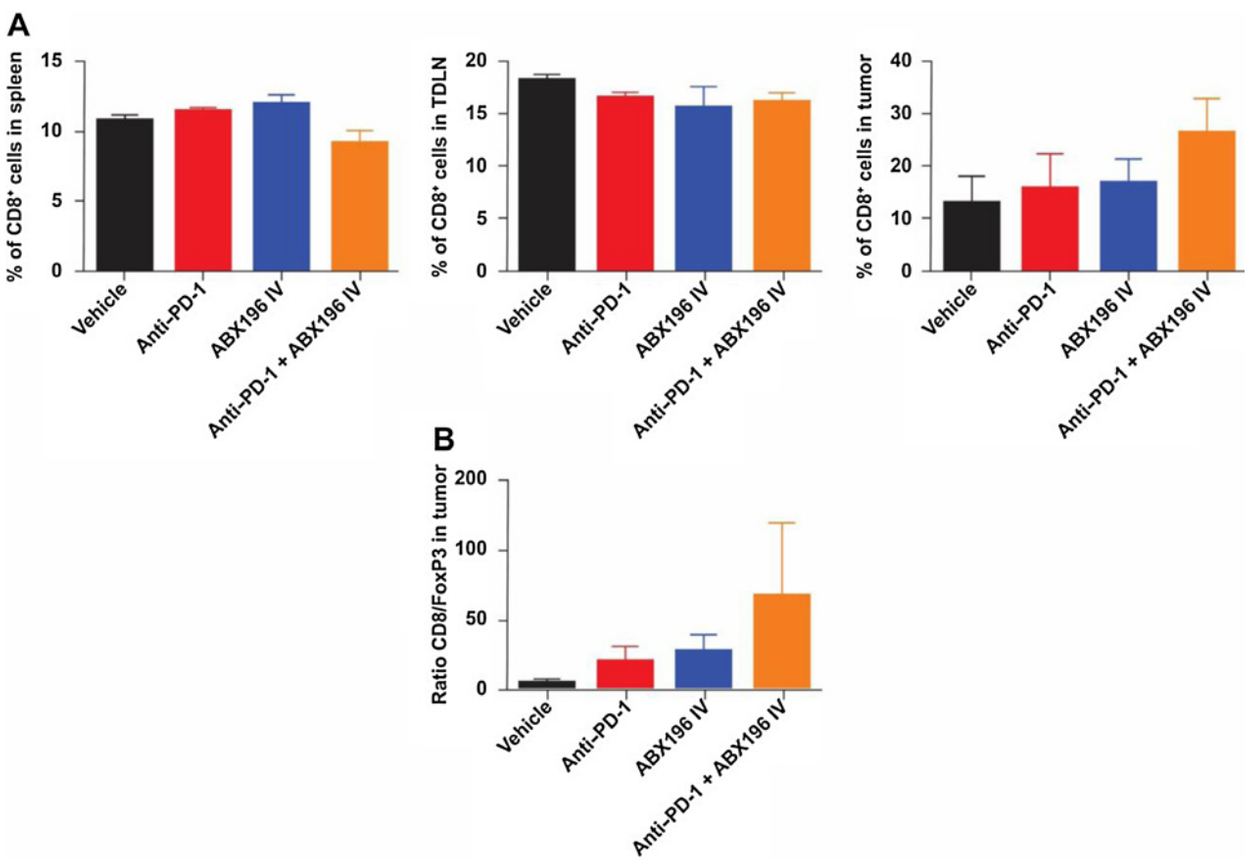

Figure 3.

Flow cytometry evaluation of $CD8^+$ cell measurements and CD8/FoxP3 ratio. **A,** Evaluation of $CD8^+$ cell frequencies in $CD45^+$ cells by flow cytometry. Spleen ($n = 6$ per group), TDLNs ($n = 6$ per group) and tumor ($n = 2/3$ per group) were harvested at day 14 from B16F10–tumor-bearing mice treated with vehicle, anti–PD-1 alone, ABX196 (100 ng), or anti–PD-1 + ABX196 (100 ng). Results were expressed as percentage of cells (mean ± SEM). **B,** Evaluation of CD8/FoxP3 ratio. Tumors ($n = 2/3$ per group) were harvested at day 14 from B16F10–tumor-bearing mice treated with vehicle, anti–PD-1 alone, ABX196 (100 ng), or anti–PD-1 + ABX196 (100 ng). Results were expressed as ratio value.

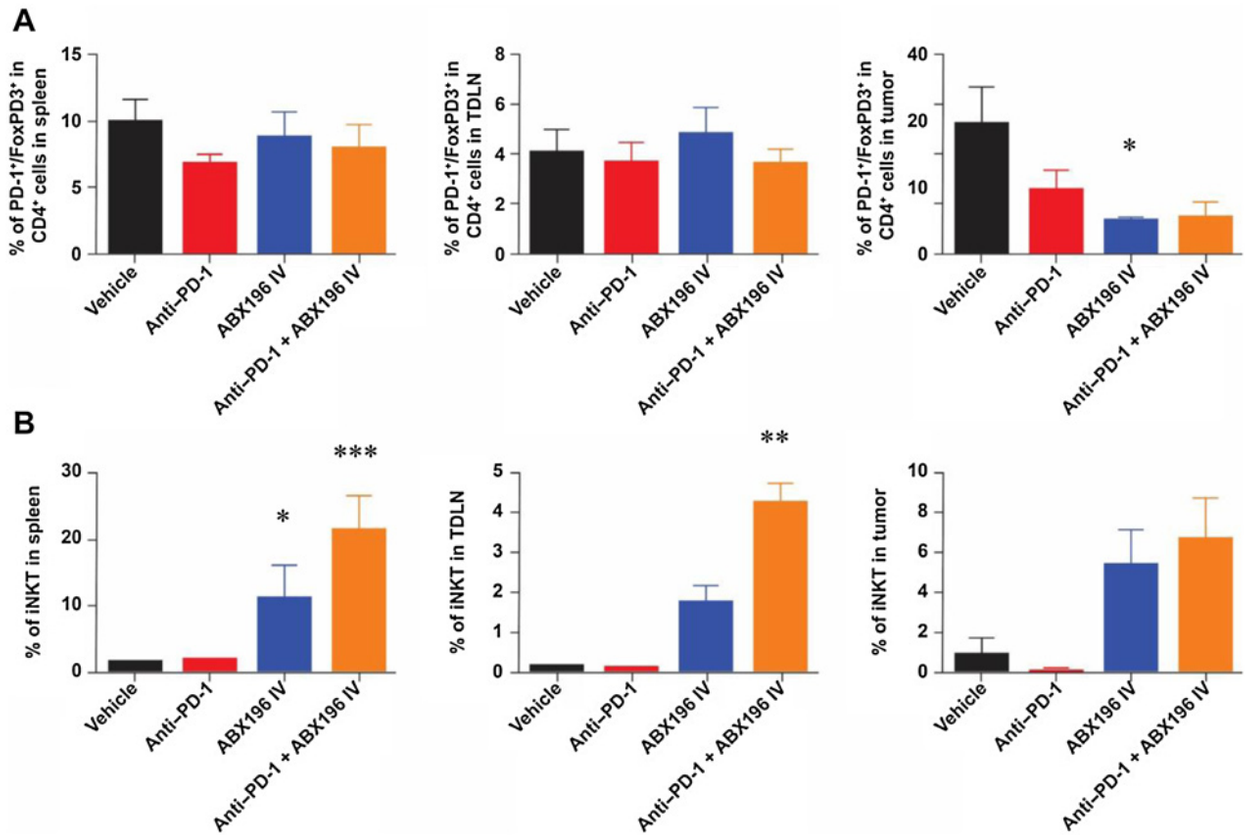

Figure 4.

Flow cytometry analysis of PD-1$^+$/FoxP3$^+$ cell frequencies and CD1d$^+$ cell frequencies. **A,** Evaluation of PD-1$^+$/FoxP3$^+$ cell frequencies in CD4$^+$ cells by flow cytometry. Spleen ($n = 6$ per group), TDLNs ($n = 6$ per group) and tumor ($n = 2/3$ per group) were harvested at day 14 from B16F10–tumor-bearing mice treated with vehicle, anti–PD-1 alone, ABX196 (100 ng), or anti–PD-1 + ABX196 (100 ng). Percentage of CD4$^+$ regulatory T significantly decreased in tumors following treatment with ABX196 (*, $P < 0.05$ vs. control, Kruskal–Wallis test). **B,** Evaluation of in CD45$^+$/CD3$^+$/CD19$^-$ cells by flow cytometry, spleen ($n = 6$ per group), TDLNs ($n = 6$ per group), and tumor ($n = 3$ per group) were harvested at day 14 from B16F10–tumor-bearing mice treated with vehicle, anti–PD-1 alone, ABX196 (100 ng), or anti–PD-1 + ABX196 (100 ng). There was a significant increase in the percentage of iNKT cells expressing CD1d markers versus control in spleen (*, $P < 0.05$, Kruskal–Wallis test). A synergistic effect was observed following combined ABX196/anti–PD-1 treatment versus control in spleen and TDLN (***, $P < 0.001$ and **, $P < 0.005$, respectively, Kruskal–Wallis test). Results were expressed as percentage of cells (mean ± SEM).

combined treatment (**Fig. 4A**). This treatment effect on Tregs was not seen in spleen and TDLNs (**Fig. 4A**). Further analysis was performed to determine the treatment effect on the concentration of NKT cells expressing CD1d markers. Following ABX196 administration, there was a significant increase in the percentage of iNKT cells expressing CD1d markers (CD45$^+$/CD3$^+$/CD19$^-$cells) versus control in spleen ($P < 0.05$), while the increase did not reach statistical significance versus control in TDLNs and tumoral tissue (**Fig. 4B**). Moreover, a synergistic effect was observed following combined ABX196/anti–PD-1 treatment in spleen ($P < 0.001$ vs. control) and TDLN ($P < 0.005$ vs. control) tissues.

Antitumor responses in the orthotopic hepa 1–6 hepatocarcinoma mouse model

A significant improvement in survival was observed following treatment with ABX196 and anti–PD-1 ($P < 0.005$ vs. control; **Fig. 5A**) as well as following combined ABX196/anti–PD-1 treatment ($P < 0.001$ vs. control; $P < 0.01$ vs. sorafenib treatment alone; Supplementary Table S2). Combined treatment with ABX196 and sorafenib resulted in significant improvement in survival ($P < 0.005$ vs. control; $P < 0.01$ vs. sorafenib alone). In mice treated with sorafenib alone, there was no significant effect on survival versus control. No significant differences in survival were seen following combined ABX196/anti–PD-1 treatment versus anti–PD-1 alone or ABX196 alone.

At study termination, liver weight—expressed as a percentage of body weight—was significantly lower for combined ABX196/anti–PD-1 treatment versus control and versus sorafenib ($P < 0.05$ for both, **Fig. 5B**). No significant effect in liver weight was observed versus control following sorafenib alone or combined ABX196/sorafenib treatment. MRI was used to further evaluate tumor invasion of the liver (Supplementary Fig. S2). Compared with control, significant reductions in metastatic invasion were observed following treatment with ABX196 ($P < 0.01$), anti–PD-1 ($P < 0.01$), combined ABX196/anti–PD-1 treatment ($P < 0.001$) and combination of ABX196 and sorafenib ($P < 0.01$; **Fig. 5C**; Supplementary Table S3). There was no significant difference in metastasis following treatment with sorafenib versus control.

Evaluation of serum IFNγ production demonstrated a synergistic effect following combined ABX196/anti–PD-1 treatment (**Fig. 6**). On day 9, the vehicle control group and anti–PD-1—treated group had

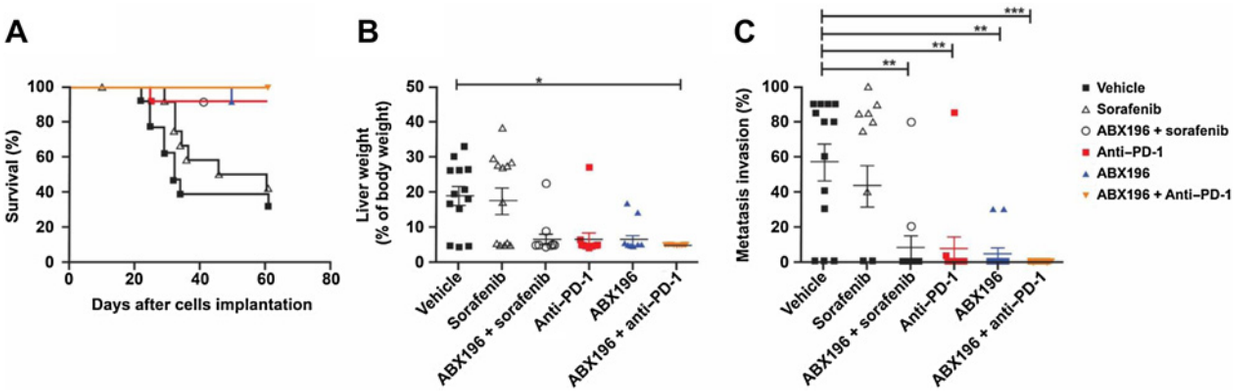

Figure 5.

Evaluation of ABX196 alone or in combination with anti–PD-1 or sorafenib on HCC. **A,** Survival analysis of C57BL/6 mice bearing OT Hepa 1–6 tumors exposed to vehicle ($n = 13$), sorafenib ($n = 13$), ABX196 alone ($n = 13$), anti–PD-1 ($n = 12$), ABX196 combined with sorafenib ($n = 12$) or to ABX196 combined with anti–PD-1 ($n = 12$). A significant improvement in survival was observed versus control following treatment with either ABX196 or anti–PD-1 monotherapy and following combined ABX196/anti–PD-1 treatment (see Supplementary Table S2 for details). **B,** Mean liver weight as percentage of body weight of C57BL/6 mice bearing OT Hepa 1–6 tumors at the time of termination exposed to the treatments described for **Fig. 4A**. Liver weight was significantly lower (*, $P < 0.05$ vs. control) for combined ABX196/anti–PD-1 treatment and sorafenib monotherapy. **C,** Evaluation of invasion of the liver by a semiquantitative analysis following visual inspection of 20 consecutive MRI pictures of 5 mice from each treatment group (as described for **Fig. 4A**). The results are expressed as a percentage of invasion. Compared with control, significant reductions in metastatic invasion were observed following treatment with either ABX196 or anti–PD-1 (**, $P < 0.01$), combination ABX196 and sorafenib (**, $P < 0.01$) and combined ABX196/anti–PD-1 treatment (***, $P < 0.001$) (see Supplementary Table S3 for details).

nonquantifiable concentrations of serum IFNγ (below 188 pg/mL). The ABX196 and combined ABX196/anti–PD-1 treatment groups had a mean IFNγ concentration of 6.95 ng/mL and 19.23 ng/mL, respectively, which both were significantly higher than control ($P < 0.0005$ and $P < 0.0001$, respectively).

Histopathologic assessment of H&E stained liver sections demonstrated tumor progression among the treatment and vehicle control groups. The stained sections from the vehicle control group showed substantial metastasis present compared with the ABX196 and anti–PD-1 treatment groups (**Fig. 7A**). In addition, immunofluorescent staining of liver tissue following incubation with the Ki-67 antibody demonstrated high concentrations of actively proliferating tumors in the livers of vehicle control–treated mice versus the ABX196 and combined ABX196/anti–PD-1 treatment groups (**Fig. 7B**).

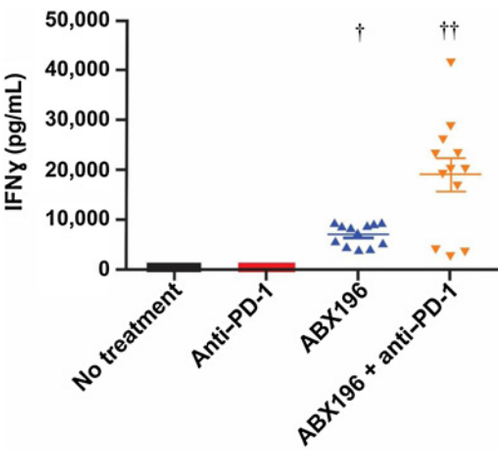

Figure 6.

IFNγ concentration (mean ± SEM) in the serum of C57BL/6J mice bearing Hepa 1–6 tumors on day 9. Animals were randomized on day 7, treated during the day 7 to day 17 period, and last mice were sacrificed on day 56. IFNγ concentrations were below the quantifiable limit of 94 pg/ml on day 3, with the exception of one mouse, which had an IFNγ concentration of 101 pg/mL. On day 9, the vehicle control group and anti–PD-1—treated group had nonquantifiable concentrations, below 188 pg/mL. The ABX196 and combined ABX196/anti–PD-1 treatment groups had a mean IFNγ concentration of 6.95 ng/mL and 19.23 ng/mL, respectively, which both were significantly higher than control (†, $P < 0.0005$ and ††, $P < 0.0001$, respectively, Kruskal–Wallis test).

Immune marker analysis through IHC was performed to further study immunologic pathways involved in ABX196-mediated antitumor activity. In the vehicle control group, the liver cell population was predominantly PD-1$^+$ cells and FoxP3$^+$ cells, reflecting the unresponsive immunologic status of this treatment group (Fig. **8**). Similarly, high levels of PD-1$^+$ and FoxP3$^+$ cells were also observed in the sorafenib treatment group. In contrast, the ABX196 treatment group demonstrated increased recruitment of F4/80$^+$ cells. The anti–PD-1 treatment group showed enhanced infiltration of PD-1$^+$ cells and decreased CD8$^+$ cell recruitment. Combined ABX196/anti–PD-1 treatment resulted in a decrease of PD-L1$^+$, PD-1$^+$, and FoxP3$^+$ cells and increased recruitment of CD4$^+$ cells.

Discussion

The major goal of immunotherapy is to induce potent antitumor T-cell responses. It is reported that the enhancement of effector T cells is most efficient with a combination of ICBs and stimulation with a potent immunomodulatory such as a Toll-like receptor agonist (9, 25). The present findings from the melanoma model study demonstrated that anti–PD-1 antibody treatment had little to no effect on tumor volume and survival endpoints. This agrees with a number of studies which report that blockade of the PD-1 pathway has little effect on melanomas (26, 27). A transient positive effect of ABX196 monotherapy was observed after 15 days for melanoma tumor volume and survival, and the combination treatment with ABX196 and anti–PD-1 resulted in a significant synergistic antitumor effect compared with other treatments and the control vehicle. This result is consistent with a preclinical B16 melanoma model study evaluating the concurrent blockade of PD-1 and CTLA-4 pathways, which led to enhanced

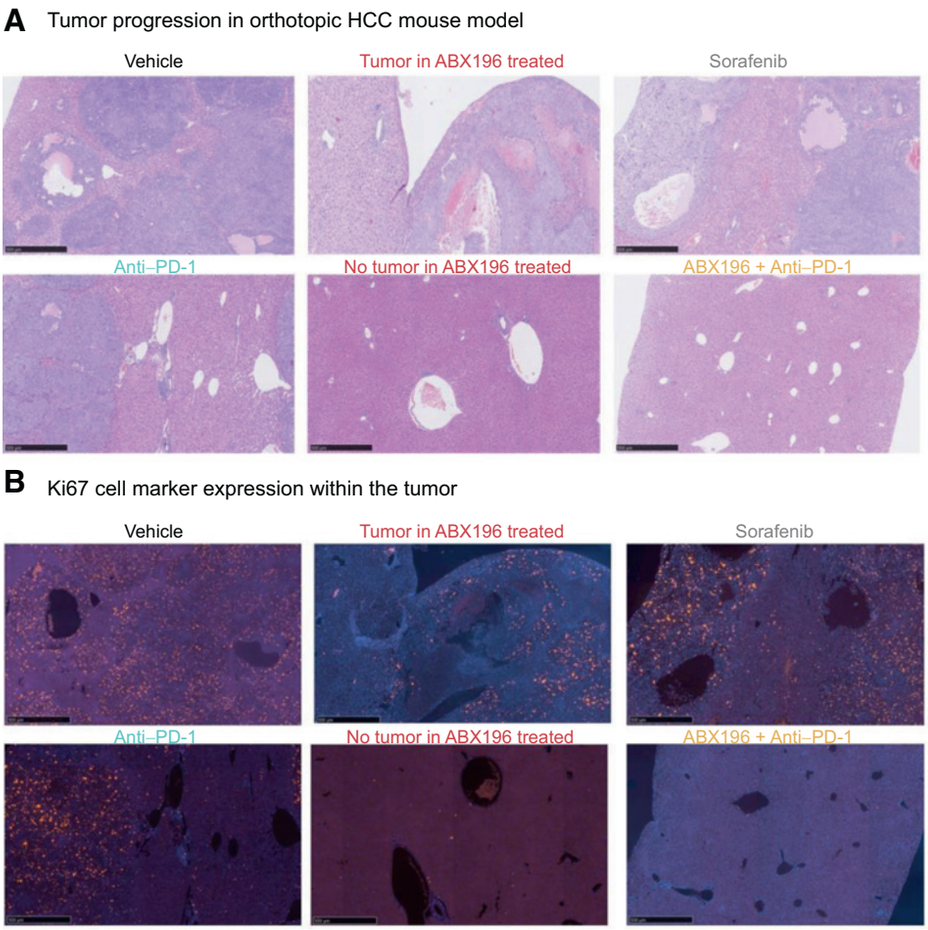

Figure 7.
H&E and immunofluorescent staining of liver tissue of C57BL/6 mice bearing OT Hepa 1–6 tumors. **A,** H&E staining of liver tissue of C57BL/6 mice bearing OT Hepa 1–6 tumors exposed to treatment with vehicle, ABX196, sorafenib, anti–PD-1 or combined ABX196 with anti–PD-1 (magnification X5). **B,** Immunofluorescent staining of liver tissue of C57BL/6 mice bearing OT Hepa 1–6 tumors following incubation with the Ki67 antibody (magnification X5). Treatments were carried as described for **Fig. 5A**.

activation marker expression and inflammatory cytokine expression following combination antibody treatment with the ratio of $CD8^+$ cells relative to Tregs and myeloid-derived suppressor cells doubled compared with single antibody treatment and more than 10-fold higher compared with the control (26). Similarly, we observed an increased percentage of $CD8^+$ cells and an increased ratio of $CD8^+$ effector cells to $FoxP3^+$ Treg cells in tumoral tissue following combined ABX196/anti–PD-1 treatment. It is not clear why this effect was only seen in tumoral tissue and not in spleen and TDLNs, but it may be related to the timing of sampling, as an increased $CD8^+$ population may not have been detectable due to CD8 apoptosis or simply due to directed relocalization of effector cells to the tumor site. Evaluation of the Treg $FoxP3^+$ cell population co-expressing the co-inhibitory PD-1 molecule further elucidated the mechanism of ABX196 and anti–PD-1 therapy. It has been previously reported that inhibition of PD-1 with a specific antibody decreased $FoxP3^+$ regulatory cells and increased $CD8^+$ T cells proliferation and tumor killing in CT26 tumor cell–bearing mice (25). In the melanoma model, we found that ABX196 substantially

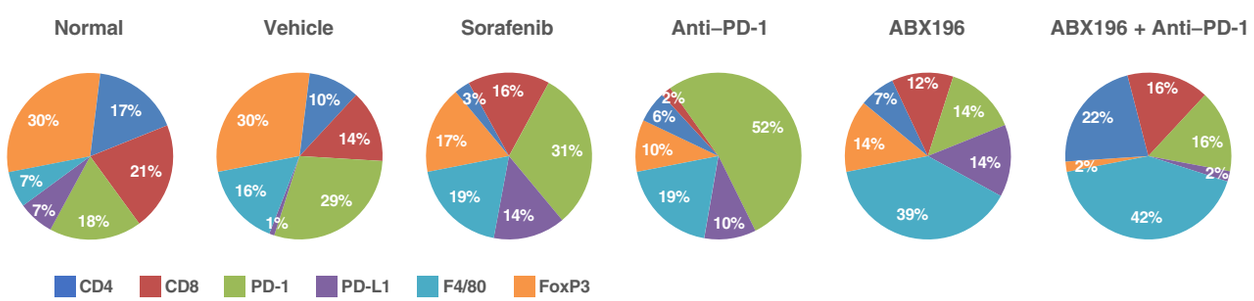

Figure 8.
Immune cell infiltration profiles in liver of C57BL/6 mice bearing OT Hepa 1–6 tumors. Immune cell infiltration profiles in liver of C57BL/6 mice bearing OT Hepa 1–6 tumors exposed to vehicle ($n = 13$), sorafenib ($n = 13$), ABX196 alone ($n = 13$), anti-PD-1 alone ($n = 12$), ABX196 combined with sorafenib ($n = 12$) or to ABX196 combined with anti-PD-1 ($n = 12$). Normal tissue is included as control.

reduced Tregs compared with control, though no synergistic effect was seen following combined therapy. The specific mechanism of ABX196 immunomodulation is associated with the activation and/or proliferation of iNKT cells, expressing a highly restricted T-cell receptor and responding to lipid ligands through CD1d restriction (18). Thereby, iNKT cells are important players governing the innate and adaptive immune response and surveilling tumors (18). This analysis demonstrated that ABX196 monotherapy increased the ratio of iNKT cell population in the spleen, tumoral tissue, and TLDNs. In addition, combined ABX196/anti–PD-1 treatment resulted in an enhanced $CD1d^+$ cell response versus ABX196 monotherapy. This series of biological effects is likely explained by the direct blockade of PD-1 on NKT cells that rescues them for undergoing poststimulation apoptosis and/or anergy. This particular mechanism exposes the limitations of using ABX196 alone. Indeed, monotherapy is followed by a 4- to 6-week-long period of NKT cell unresponsiveness that can only be overcome by a long spacing of injections.

Immune tolerance that characterizes the evolution of HCC is regulated by innate and adaptive immune cells present in the immune tumor microenvironment such as $CD4^+$ and $CD8^+$ T cells, dendritic cells, NK cells, myeloid-derived suppressor cells, tumor-associated macrophages that express and up-regulate immune checkpoints on their surface (28, 29). Increased $FoxP3^+$ cell infiltration in HCC tumors has been reported to be associated with worse patient survival (30–33), indicating this malignancy may be a promising target for immunomodulation therapy (34). In the mouse model transplanted with Hepa 1–6 cell line, combined ABX196/anti–PD-1 treatment led to significant improvements in survival, metastasis invasion, and liver weight, while combination treatment with ABX196 and sorafenib significantly improved survival and reduced metastatic invasion. In addition, monotherapy with either ABX196 or anti–PD-1 significantly improved survival and decreased metastatic invasion compared with vehicle control. No significant differences in survival were seen following combined ABX196/anti–PD-1 treatment vs. anti–PD-1 alone or ABX196 alone, most likely because of the high level of survival already obtained after single treatment with either therapy. It is hypothesized that a synergistic effect of the combined therapy might be evidenced by decreasing the doses of ABX196 and anti–PD-1. However, a synergistic effect of combined ABX196/anti–PD-1 treatment was apparent when IFNγ was measured in peripheral blood, indicating sustained activation of iNKT cells and probably transactivation of different cell types known to produce IFNγ, such as NKT cells (35). The pattern of response to treatment was confirmed using MR imaging. Significant reductions in tumor invasion were achieved by ABX196 monotherapy, anti–PD-1 monotherapy, combined ABX196/anti–PD-1 treatment, and combined ABX196/sorafenib treatment versus vehicle control. These results were further supported by histopathologic analysis of liver sections.

Moreover, the most frequent cell populations seen in vehicle-treated mice expressed $FoxP3^+$ and $PD\text{-}1^+$ markers, reflecting tumor-induced proliferation and accumulation of cells that result in T-cell anergy. Interestingly, cell populations from the sorafenib-treated group similarly expressed high levels of $FoxP3^+$ and $PD\text{-}1^+$ markers. ABX196 treatment increased recruitment of $F4/80^+$ cells, thereby enhancing dendritic cell activity and inflammatory responses (36, 37). The types of tumor associated macrophage that were recruited in the tumor microenvironment of HCC treated with ABX196+anti–PD-1 were not specifically determined. It may be relevant to perform such analysis in the near future, as several studies have shown the ability of iNKT cells to reshape suppressive myelomonocytic populations in the tumor microenvironment (38). ABX196 treatment also augmented the proportion of $PD\text{-}L1^+$ cells by 2-fold compared with vehicle control. Adaptive PD-L1 upregulation is reported to be a consequence of an inflammatory cytokine milieu caused by tumor-associated macrophages and/or IFNγ (30), and may be a favorable prognostic factor for some cancers (39, 40). In this study, anti–PD-1 enhanced the frequency of PD-1 cells and decreased the percentage of $CD8^+$ cells in the liver. The latter decrease is difficult to understand but we hypothesize it could be a consequence of an increased expression of PD-1 or increased infiltration of PD-1 cells into the tumor, decreasing the percentage of $CD8^+$ cells but not their absolute number. Combination treatment with ABX196 and anti–PD-1 resulted in a substantial reduction in the percentage of $FoxP3^+$, $PD\text{-}1^+$, and $PD\text{-}L1^+$ cells, and increased recruitment of $CD4^+$ cells. This immune profile reflected a general shifting of the tumor microenvironment from suppressive to inflammatory, with an increase in effector cells and decrease in Treg cells.

In summary, investigations of ABX196 with anti–PD-1 in the B16F10 mouse melanoma model demonstrated a synergistic antitumor effect with combined use, with the ratio of CD8 effector to FoxP3 Tregs in tumor tissue being highest after combined administration of anti–PD-1 and ABX196. Both mouse melanoma and HCC models demonstrate that the antitumor effects were associated with a generation of a more advantageous T-effector to Treg cell ratio within the tumor, which could lead to the proliferation and accumulation of cells that would otherwise be anergized. ABX196 plus anti–PD-1 antibody may be a novel strategy to overcome the immunosuppressive microenvironment and to produce antitumor activity. Pre-administration of anti–PD-1 antibodies prevented α-GalCer–induced iNKT cell anergy and may also enhance iNKT cell–induced T-cell response (41).

The current data provide the scientific basis for human clinical trials that would involve a combination of ABX196 with ICBs. Of course, caution should be exercised when interpreting some of the results, especially in terms of their transferability to humans. Important differences exist between clinical reality and certain experimental conditions and/or animal models. For example, iNKT cells represent 20% to 30% of T cells in the mouse liver, yet only 0.5% to 0.8% of T cells in the human liver (35), so there is no guarantee that similar results will be observed in humans. A phase I clinical study was approved by the FDA to evaluate the combination of ABX196 and the anti–PD-1 antibody nivolumab for the treatment of HCC. In a small but heavily pretreated HCC population, ABX196 plus nivolumab was well tolerated and initial results of clinical benefit warrant the continued clinical development of ABX196 in patients with HCC as a strategy to overcome the immunosuppressive microenvironment in this disease (42).

Authors' Disclosures

L. Teyton reports other support from Abivax during the conduct of the study; in addition, L. Teyton has a patent for US8207135 issued. T. Pearce reports personal fees from Abivax during the conduct of the study. P. Pouletty reports other support from Abivax outside the submitted work; in addition, P. Pouletty has a patent for Patent issued; and member of the board of directors of Abivax, CEO of Truffle Capital, Abivax shareholder. H.J. Ehrlich reports a patent for Abivax intraperitoneal issued; and Abivax CEO. No disclosures were reported by the other authors.

Authors' Contributions

D. Scherrer: Conceptualization, resources, data curation, formal analysis, supervision, validation, investigation, methodology, writing–original draft, writing–review and editing. **N. Barrett:** Conceptualization, resources, data curation, formal analysis, supervision, validation, investigation, methodology, writing–original draft, writing–

review and editing. **L. Teyton:** Supervision, writing–original draft, writing–review and editing. **T. Pearce:** Supervision, writing–original draft, writing–review and editing. **J. Nitcheu:** Investigation. **P. Pouletty:** Resources, supervision, funding acquisition. **J. Santo:** Formal analysis, methodology, writing–review and editing. **H.J. Ehrlich:** Conceptualization, supervision, validation, methodology.

Acknowledgments

This study was funded by Abivax.

The authors would like to thank S. Crabé on behalf of Abivax, for her assistance in preparing the manuscript.

The publication costs of this article were defrayed in part by the payment of publication fees. Therefore, and solely to indicate this fact, this article is hereby marked "advertisement" in accordance with 18 USC section 1734.

Note

Supplementary data for this article are available at Molecular Cancer Therapeutics Online (http://mct.aacrjournals.org/).

Received March 15, 2022; revised July 26, 2022; accepted September 28, 2022; published first October 5, 2022.

References

1. Fitzmaurice C, Akinyemiju TF, Al Lami FH, Alam T, Alizadeh-Navaei R, Allen C, et al. Global, regional, and national cancer incidence, mortality, years of life lost, years lived with disability, and disability-adjusted life-years for 29 cancer groups, 1990 to 2016: a systematic analysis for the global burden of disease study. JAMA Oncol 2018;4:1553–68.
2. Sung H, Ferlay J, Siegel RL, Laversanne M, Soerjomataram I, Jemal A, et al. Global cancer statistics 2020: GLOBOCAN estimates of incidence and mortality worldwide for 36 cancers in 185 countries. CA Cancer J Clin 2021;71:209–49.
3. El-Serag HB. Epidemiology of viral hepatitis and hepatocellular carcinoma. Gastroenterology 2012;142:1264–73.
4. El-Khoueiry A. The promise of immunotherapy in the treatment of hepatocellular carcinoma. Am Soc Clin Oncol Educ Book 2017;37:311–7.
5. Chen DS, Mellman I. Oncology meets immunology: the cancer-immunity cycle. Immunity 2013;39:1–10.
6. Koebel CM, Vermi W, Swann JB, Zerafa N, Rodig SJ, Old LJ, et al. Adaptive immunity maintains occult cancer in an equilibrium state. Nature 2007;450:903–7.
7. Smyth MJ, Dunn GP, Schreiber RD. Cancer immunosurveillance and immunoediting: the roles of immunity in suppressing tumor development and shaping tumor immunogenicity. Adv Immunol 2006;90:1–50.
8. Hernandez-Gea V, Toffanin S, Friedman SL, Llovet JM. Role of the microenvironment in the pathogenesis and treatment of hepatocellular carcinoma. Gastroenterology 2013;144:512–27.
9. Butt AQ, Mills KH. Immunosuppressive networks and checkpoints controlling antitumor immunity and their blockade in the development of cancer immunotherapeutics and vaccines. Oncogene 2014;33:4623–31.
10. Nishikawa H, Sakaguchi S. Regulatory T cells in cancer immunotherapy. Curr Opin Immunol 2014;27:1–7.
11. Pardoll DM. The blockade of immune checkpoints in cancer immunotherapy. Nat Rev Cancer 2012;12:252–64.
12. Martini G, Ciardiello D, Paragliola F, Nacca V, Santaniello W, Urraro F, et al. How immunotherapy has changed the continuum of care in hepatocellular carcinoma. Cancers 2021;134719.
13. Larkin J, Chiarion-Sileni V, Gonzalez R, Grob JJ, Cowey CL, Lao CD, et al. Combined nivolumab and ipilimumab or monotherapy in untreated melanoma. N Engl J Med 2015;373:23–34.
14. Sidaway P. Bladder cancer: atezolizumab effective against advanced-stage disease. Nat Rev Urol 2016;13:238.
15. Topalian SL, Drake CG, Pardoll DM. Immune checkpoint blockade: a common denominator approach to cancer therapy. Cancer Cell 2015;27:450–61.
16. Tefit JN, Crabé S, Orlandini B, Nell H, Bendelac A, Deng S, et al. Efficacy of ABX196, a new NKT agonist, in prophylactic human vaccination. Vaccine 2014;32:6138–45.
17. Freigang S, Landais E, Zadorozhny V, Kain L, Yoshida K, Liu Y, et al. Scavenger receptors target glycolipids for natural killer T-cell activation. J Clin Invest 2012;122:3943–54.
18. Juno JA, Keynan Y, Fowke KR. Invariant NKT cells: regulation and function during viral infection. PLoS Pathog 2012;8:e1002838.
19. Gumperz JE, Miyake S, Yamamura T, Brenner MB. Functionally distinct subsets of CD1d-restricted natural killer T cells revealed by CD1d tetramer staining. J Exp Med 2002;195:625–36.
20. Matsuda JL, Mallevaey T, Scott-Browne J, Gapin L. CD1d-restricted iNKT cells, the 'Swiss-Army knife' of the immune system. Curr Opin Immunol 2008;20:358–68.
21. Galli G, Pittoni P, Tonti E, Malzone C, Uematsu Y, Tortoli M, et al. Invariant NKT cells sustain specific B cell responses and memory. Proc Natl Acad Sci USA. 2007;104:3984–9.
22. Xie B, Wang DH, Spechler SJ. Sorafenib for treatment of hepatocellular carcinoma: a systematic review. Dig Dis Sci 2012;57:1122–9.
23. Scholzen T, Gerdes J. The Ki-67 protein: from the known and the unknown. J Cell Physiol 2000;182:311–22.
24. Yerushalmi R, Woods R, Ravdin PM, Hayes MM, Gelmon KA. Ki67 in breast cancer: prognostic and predictive potential. Lancet Oncol 2010;11:174–83.
25. Dyck L, Wilk MM, Raverdeau M, Misiak A, Boon L, Mills KH. Anti–PD-1 inhibits Foxp3(+) Treg cell conversion and unleashes intratumoral effector T cells thereby enhancing the efficacy of a cancer vaccine in a mouse model. Cancer Immunol Immunother 2016;65:1491–8.
26. Curran MA, Montalvo W, Yagita H, Allison JP. PD-1 and CTLA-4 combination blockade expands infiltrating T cells and reduces regulatory T and myeloid cells within B16 melanoma tumors. Proc Natl Acad Sci USA 2010;107:4275–80.
27. Hu Z, Ye L, Xing Y, Hu J, Xi T. Combined SEP and anti–PD-L1 antibody produces a synergistic antitumor effect in B16-F10 melanoma-bearing mice. Sci Rep 2018;8:217.
28. Fu Y, Liu S, Zeng S, Shen H. From bench to bed: the tumor immune microenvironment and current immunotherapeutic strategies for hepatocellular carcinoma. J Exp Clin Cancer Res 2019;38:396.
29. Kurebayashi Y, Ojima H, Tsujikawa H, Kubota N, Maehara J, Abe Y, et al. Landscape of immune microenvironment in hepatocellular carcinoma and its additional impact on histological and molecular classification. Hepatology 2018;68:1025–41.
30. Chen J, Feng Y, Lu L, Wang H, Dai L, Li Y, et al. Interferon-γ–induced PD-L1 surface expression on human oral squamous carcinoma via PKD2 signal pathway. Immunobiology 2012;217:385–93.
31. Chen KJ, Zhou L, Xie HY, Ahmed TE, Feng XW, Zheng SS. Intratumoral regulatory T cells alone or in combination with cytotoxic T cells predict prognosis of hepatocellular carcinoma after resection. Med Oncol 2012;29:1817–26.
32. Fu J, Xu D, Liu Z, Shi M, Zhao P, Fu B, et al. Increased regulatory T cells correlate with CD8 T-cell impairment and poor survival in hepatocellular carcinoma patients. Gastroenterology 2007;132:2328–39.
33. Kobayashi N, Hiraoka N, Yamagami W, Ojima H, Kanai Y, Kosuge T, et al. $FOXP3^{+}$ regulatory T cells affect the development and progression of hepatocarcinogenesis. Clin Cancer Res 2007;13:902–11.
34. Federico P, Petrillo A, Giordano P, Bosso D, Fabbrocini A, Ottaviano M, et al. Immune checkpoint inhibitors in hepatocellular carcinoma: current status and novel perspectives. Cancers 2020;12:3025.
35. Bendelac A, Savage PB, Teyton L. The biology of NKT cells. Annu Rev Immunol 2007;25:297–336.
36. Lin HH, Faunce DE, Stacey M, Terajewicz A, Nakamura T, Zhang-Hoover J, et al. The macrophage F4/80 receptor is required for the induction of antigen-specific efferent regulatory T cells in peripheral tolerance. J Exp Med 2005;201:1615–25.
37. Lin HH, Stacey M, Stein-Streilein J, Gordon S. F4/80: the macrophage-specific adhesion-GPCR and its role in immunoregulation. Adv Exp Med Biol 2010;706:149–56.
38. Ikarashi Y, Mikami R, Bendelac A, Terme M, Chaput N, Terada M, et al. Dendritic cell maturation overrules H-2D-mediated natural killer T (NKT) cell inhibition: critical role for B7 in CD1d-dependent NKT cell interferon gamma production. J Exp Med 2001;194:1179–86.

39. Kim HR, Ha SJ, Hong MH, Heo SJ, Koh YW, Choi EC, et al. PD-L1 expression on immune cells, but not on tumor cells, is a favorable prognostic factor for head and neck cancer patients. Sci Rep 2016;6:36956.
40. Zhao T, Li C, Wu Y, Li B, Zhang B. Prognostic value of PD-L1 expression in tumor infiltrating immune cells in cancers: a meta-analysis. PLoS One 2017;12: e0176822.
41. Parekh VV, Lalani S, Kim S, Halder R, Azuma M, Yagita H, et al. PD-1/PD-L blockade prevents anergy induction and enhances the antitumor activities of glycolipid-activated invariant NKT cells. J Immunol 2009;182:2816–26.
42. Sigal D, Bhangoo MS, Frenette CT, Lee SS, Fark C, Gineste P, et al. A phase I study of ABX196 in combination with nivolumab in patients with previously treated hepatocellular carcinoma (HCC). J Clin Oncol 2022;40:429.